

Modeling Proton Mobility in Acidic Zeolite Clusters. 3. A Sudden Approximation via Semiclassical Rate Theory[†]

Justin T. Fermann[‡] and Scott M. Auerbach^{*,‡,§}

Departments of Chemistry and of Chemical Engineering, University of Massachusetts, Amherst, Massachusetts 01003

Received: October 17, 2000; In Final Form: January 30, 2001

We have developed and applied an angular sudden approximation for modeling proton transfer in zeolites, using Miller's semiclassical transition state theory. We have parametrized the rate theory by performing B3LYP/6-311G(d,p) density functional theory calculations for paths with fixed O–Al–O angle in a cluster model of H–Y zeolite. We find that both the barrier height and barrier curvature increase with O–Al–O angle. We also find that the classical barrier height increases with angle more rapidly than does the curvature, forcing the tunneling probability to decrease strongly with angle. The range of important angles for proton transfer, the so-called dynamical distribution, involves angles far from the saddle point angle at low temperatures (i.e., large curvature paths), and broadens significantly at higher temperatures, encompassing the saddle point region. The final temperature dependence of the proton jump rate within the sudden approximation shows surprisingly good agreement with that from conventional semiclassical transition state theory, which is based on the minimum energy path. We attribute this in part to a coincidence that occurs in the temperature regime of interest, namely 200–1000 K, a coincidence that we do not expect will occur in other systems.

I. Introduction

Zeolites are nanoporous, shape-selective catalysts widely used in the chemical industry for applications ranging from petroleum cracking to fine chemical synthesis.^{1,2} Many reactions begin with proton transfer from zeolite Brønsted acid sites $\equiv\text{Si}-\text{OH}-\text{Al}\equiv$. Acidic zeolites thus provide a fascinating and important platform for modeling condensed phase proton transfer, without the difficulty of sampling solvent reorganization as occurs in liquids. However, despite the relative simplicity of proton transfer in zeolites, the fundamental reaction dynamics of these systems are poorly known. Recent attempts at calculating zeolitic proton jump rates have focused almost³ exclusively on paths that intersect the transition state, i.e., the first-order saddle point separating reactants from products.^{3–6} Such approaches tacitly assume that the zeolite framework equilibrates to the motion of an activated proton. However, the reverse seems more likely, namely that the proton jump is rapid compared to time scales of framework relaxation.⁷ In this article, which builds directly on our previous work,^{4,5} we apply quantum chemistry and semiclassical rate theory to the development of a sudden approximation for proton transfer in model zeolite clusters.

To calculate rates of proton transfer in zeolites, one has to develop approximate representations for the zeolite framework, the electronic structure and the nuclear dynamics. In a previous article, denoted paper I, we focused on small cluster models in order to approach convergence of the electronic wave function.⁴ We found that using the B3LYP density functional^{8,9} with basis sets of triple- ζ quality in the valence space, and including polarization functions on all atoms, is the most efficient method for converging structures and vibrational frequencies. For

converging classical barrier heights to within ~ 1 kcal mol⁻¹, we found it necessary to augment MP2 barrier heights calculated using large basis sets with MP4 energies obtained in more limited basis sets.^{10,11} The need to apply such high levels of theory precludes the calculation of reasonably complete potential energy surfaces for these high-dimensional systems, as would be required in many quantum rate theories.^{12,13} As such, we rely on "direct" dynamical methods that require a realistically limited set of potential energy parameters, because of the significant ab initio expense associated with calculating those parameters.

Over the years Miller and co-workers have made several fundamental advances in direct dynamics, most notably the reaction path Hamiltonian¹⁴ and semiclassical transition state theory (SC-TST).¹⁵ In this article we focus on the latter, which was inspired by the following key insight by Miller in 1977: one-dimensional semiclassical tunneling theory can be extended to multidimensional systems by conceiving of a generalized barrier penetration integral, θ .¹⁵ By expanding the potential energy surface in normal modes at the saddle point, Miller showed that θ is proportional to the locally conserved semiclassical action associated with harmonic barrier crossing.¹⁵ In a particularly elegant development, Miller and co-workers extended SC-TST to treat barrier anharmonicity and reaction path curvature by expanding the potential at the transition state to quartic order, and semiclassically quantizing the resulting Hamiltonian within perturbation theory.^{16,17} This approach remains one of the simplest ways to incorporate ab initio data directly into a high-quality rate theory. Unfortunately, for many complex problems of chemical and materials science interest, the cubic and quartic force constants that are required¹⁶ to parametrize this nonseparable SC-TST are impractical to obtain from electronic structure calculations. And indeed, without these anharmonicities SC-TST reduces to quantum harmonic TST, which diverges at sufficiently low temperatures. To ameliorate

[†] Part of the special issue "William H. Miller Festschrift".

* Corresponding author. E-mail: auerbach@chem.umass.edu.

[‡] Department of Chemistry.

[§] Department of Chemical Engineering.

this difficulty, we have shown in a previous article, denoted paper II, that the harmonic version of Miller's SC-TST can be stabilized by reintroducing the ground state of reactants,⁵ which is reminiscent of the truncated parabolic barrier considered by Bell in 1934.¹⁸ In this article we revisit truncated-harmonic SC-TST for use in a sudden approximation for proton transfer in zeolites.

In paper II, we applied truncated-harmonic SC-TST to proton transfer in H–Y zeolite with potential parameters calculated in paper I. For this system, Sarv et al.¹⁹ used variable temperature MAS NMR to measure proton jump rates at 298 K, 478, 568, and 658 K, yielding an apparent activation energy of 61 kJ mol⁻¹. The best electronic structure calculations in paper I predict a zero-point vibrational energy (ZPVE) corrected barrier of 86.1 kJ mol⁻¹ for proton transfer in an isolated cluster. By forcing an Arrhenius fit through SC-TST jump rates calculated at the four temperatures studied by Sarv et al., we obtained an apparent activation energy of 53.0 kJ mol⁻¹. In an effort to include some approximate measure of long-range forces, which are ignored by our cluster model, we incorporated embedded cluster energies reported by Sauer et al.²⁰ and arrived in paper I at a final ZPVE corrected barrier of 97.1 kJ mol⁻¹. In paper II we recalculated SC-TST jump rates using this augmented barrier, and subjected the results to the Arrhenius analysis at the temperatures studied by Sarv et al., arriving at an apparent activation energy of 60.3 kJ mol⁻¹. This remarkable agreement with the 61 kJ mol⁻¹ reported by Sarv et al. is likely to involve fortuitous cancellation of error in our truncated-harmonic SC-TST, since barrier anharmonicity tends to decrease tunneling probabilities, while corner-cutting tends to increase them.¹⁶ Nonetheless, this result strongly suggests that true proton-transfer barriers are being underestimated by neglecting tunneling when interpreting mobility data.

By focusing on barrier crossing dynamics near the saddle point, SC-TST clearly gives the correct high temperature limit. Indeed, even instanton theory produces the minimum energy path (MEP) for sufficiently high temperatures.^{21,22} However, for lower temperatures where tunneling dominates the jump rate, corner-cutting paths far from the MEP (i.e., large curvature paths) can become important,³ since tunneling probabilities are generally more sensitive to barrier width than they are to barrier height. In principle, nonseparable SC-TST can account for this through coupling between the reaction coordinate and orthogonal vibrations,^{16,17} although the cubic and quartic force constants that supply this coupling may not provide the most convenient representation of the underlying physics.

An alternative picture involves the proton making *sudden* jumps for various fixed zeolite framework configurations; this is motivated by the fact that the proton is light compared to the zeolite atoms. Such paths would deviate strongly from the MEP, making them large curvature paths. For proton transfer in zeolites, the most strongly coupled framework motion is the local O–Al–O bending vibration, which changes along the MEP by about 15° as it modulates the proton transfer donor–acceptor distance.^{4,6} Such a situation has already been described for proton transfer in solution; for example, see Figure 1 in ref 7 by Borgis and Hynes. An angular sudden approximation for proton transfer in zeolites would involve performing rate calculations for various fixed O–Al–O angles, and then averaging over the fixed-angle jump rates with the proper weighting. In principle, other local coordinates that couple with the proton jump could be treated in the same way. Below we pursue this sudden approximation in the language of truncated-harmonic SC-TST, with slight modifications that account for

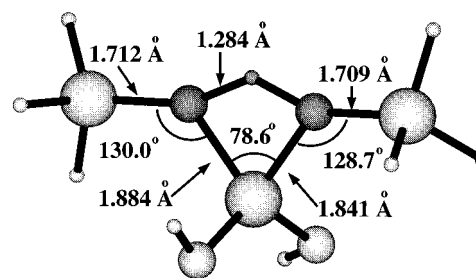


Figure 1. Cluster model of proton transfer in H–Y zeolite, showing a fixed-angle transition state very near the first-order saddle point for this system.

barrier crossing away from critical points on the potential surface. By explicitly treating corner-cutting (i.e., fixed-angle) paths with a truncated-harmonic formulation, we are relaxing one of the two partially canceling approximations made in paper II. We are thus breaking a golden rule of theoretical science: make approximations two at a time! Despite this departure from canceling approximations, we find below that the overall temperature dependence of the proton jump rate within the sudden approximation agrees surprisingly well with that from the minimum energy path calculations reported in paper II.

The remainder of this paper is organized as follows: in section II we describe the computational methods used for both electronic structure and dynamics calculations, in section III we discuss the results, and in section IV we give concluding remarks.

II. Computational Methods

In this section we begin by reviewing the molecular cluster used to study proton transfer between the O(1) and O(4) bridging oxygens in H–Y zeolite. This is followed by a description of the electronic structure methods used to parametrize the proton-transfer potential surface. We then outline the sudden approximation for proton transfer using truncated-harmonic SC-TST.

A. Zeolite Cluster Model. We model proton transfer in a zeolite cluster with H₃Si(O)Al(OH)₂OSiH₃⁻ connectivity. The underlined oxygens are the donor and acceptor, labeled O(1) and O(4), respectively. As detailed in paper I, the cluster is initially constructed by truncating a small piece of H–Y zeolite with terminal hydrogens. These are placed in the directions of the next framework atoms in the actual zeolite, at distances of 1.4 and 0.9 Å for the fabricated SiH and OH bonds, respectively. The terminal hydrogens are kept frozen in space to mimic the mechanical restraints of the zeolite framework. All remaining atoms are allowed complete geometric freedom during optimization except for the O–Al–O angle, which is frozen at various values in accord with the sudden approximation. A typical cluster is shown above in Figure 1.

B. Electronic Structure Methods. In paper I we reported a convergence study of electronic structure methods²³ showing that accurate results can be obtained efficiently for this system by first optimizing the cluster geometry with B3LYP/6-311G(d,p). Sufficiently converged electronic energies were then obtained by evaluating the MP2/6-311G(d,p) energy and adding the difference {E[MP4/6-311G(d)] – E[MP2/6-311G(d)]}.²⁴ As shown in paper I, such an approach yields a classical barrier height within 0.43 kcal mol⁻¹ of that calculated with the coupled-cluster method CCSD(T)/6-31G(d). We also found that B3LYP/6-311G(d,p) alone gives good results for geometries and frequencies but underestimates barriers by about 2.0–2.5 kcal mol for this system, which is about 10% of the classical barrier height.

For computational efficiency in the present study, we will perform only B3LYP/6-311G(d,p) calculations; these will provide qualitatively reliable, but not quantitatively accurate, trends regarding the angular dependence of proton jump potential parameters. Below we use analytic gradients to locate fixed-angle reactant minima and transition states. Analytic energy second derivatives in mass-weighted coordinates are used to evaluate harmonic vibrational frequencies. During normal-mode analysis, we set the mass of frozen hydrogens to a very large number, e.g., 10^6 au. This removes spurious imaginary frequencies associated with restraining the cluster and gives vibrational frequencies in good agreement with those observed from infrared measurements of bulk Na–Y zeolite.²⁵

All calculations were performed using GAUSSIAN98²⁴ on Intel Linux workstations. Representative calculation times for a 500 MHz Pentium III processor are B3LYP/6-311G(d,p) optimization, 15 CPU hours, and B3LYP/6-311G(d,p) frequencies, 9 CPU hours. The calculations employed direct integral methods, requiring no more than 100 megabytes of disk space.

C. Rate Theory. Our angular sudden approximation for proton transfer in zeolites entails performing rate calculations for various fixed O–Al–O angles (ϕ), and then averaging over the fixed-angle jump rates with the proper weighting. The ansatz of our angular sudden approximation is thus given by

$$k \cong \int d\phi \rho(\phi) k(\phi) \cong \sum_{j=1}^{N_\phi} \Delta\phi_j \rho(\phi_j) k(\phi_j) \quad (2.1)$$

where $\rho(\phi)$ and $k(\phi)$ are the properly normalized, ϕ -dependent probability and rate constant, respectively. To remain consistent with SC-TST, all zero-point vibrational energies (ZPVE) and summations over state space are contained within $k(\phi)$. The only average not handled within $k(\phi)$ is of course the average over ϕ itself; to accomplish this final average $\rho(\phi)$ takes the form:

$$\rho(\phi_j) = e^{-\beta V^r(\phi_j)} \left/ \sum_{j'=1}^{N_\phi} \Delta\phi_{j'} e^{-\beta V^r(\phi_{j'})} \right. \quad (2.2)$$

where $V^r(\phi_j)$ is the ground electronic energy of reactants with the O–Al–O angle set to ϕ_j .

We approximate $k(\phi)$ with truncated-harmonic SC-TST, inspired mainly by the work of Hernandez and Miller in 1993.¹⁷ We give a detailed review of Hernandez and Miller's formulation in paper II, as well as the derivation of the truncated-harmonic version of SC-TST; here we briefly review the main results. The truncated-harmonic SC-TST rate constant takes the form

$$k^{\text{SC-TST}}(T) = k^{\text{TST}}(T) \cdot \Gamma(T) = \frac{k_B T}{h} \frac{Q^\ddagger}{Q^r} \Gamma(T) \quad (2.3)$$

where $k^{\text{TST}}(T)$ is the harmonic TST rate constant and $\Gamma(T)$ is the tunneling correction factor. In eq 2.3, k_B is Boltzmann's constant, T is temperature, $h = 2\pi\hbar$ is Planck's constant, and Q^r , Q^\ddagger , and $\Gamma(T)$ are given by

$$Q^r = \sum_{n^r} \exp \left\{ -\beta \left[\Delta V^r + \sum_{i=1}^F \hbar \omega_i^r \left(n_i^r + \frac{1}{2} \right) \right] \right\} \quad (2.4)$$

$$Q^\ddagger = \sum_{n^\ddagger} \exp \left\{ -\beta \left[\Delta V^\ddagger + \sum_{i=1}^{F-1} \hbar \omega_i^\ddagger \left(n_i^\ddagger + \frac{1}{2} \right) \right] \right\} \quad (2.5)$$

$$\Gamma(T) = \frac{e^{\beta \Delta E_0}}{1 + e^{2\theta_0}} + \frac{1}{2} \int_{-\infty}^{\theta_0} d\theta e^{\beta \hbar |\omega_F^\ddagger| \theta / \pi} \text{sech}^2 \theta \quad (2.6)$$

In eqs 2.4–2.6, many physical quantities arise that require explanation. Before doing so below, we remind the reader that each of these quantities depends on the O–Al–O angle, ϕ_j . For notational brevity we omit the explicit angular dependence.

The quantities that comprise the reactant volume and dividing surface partition functions, Q^r and Q^\ddagger , respectively, are completely analogous except that Q^r samples all reactant vibrations while Q^\ddagger only samples the $F - 1$ stable vibrations at the transition state, hence the sum over $F - 1$ modes in eq 2.5. In eq 2.4, $\beta = (1/k_B T)$, $n^r = (n_1^r, n_2^r, \dots, n_F^r)$ are the $F = 48$ vibrational quantum numbers of the reactant, and $(\omega_1^r, \omega_2^r, \dots, \omega_F^r)$ are the corresponding vibrational frequencies. The quantities in eq 2.5 are defined at the transition state by analogy to eq 2.4. At the transition state the vibrational frequency of the reaction coordinate, ω_F^\ddagger , is imaginary; its corresponding quantum number was related by Miller to the generalized barrier penetration integral, θ , according to¹⁵

$$\theta = -i\pi \left(n_F^\ddagger + \frac{1}{2} \right) \quad (2.7)$$

As with one-dimensional WKB theory,²⁶ θ in eq 2.7 is a real number that vanishes at the transition state and decreases with increasing energy.

In eq 2.4, ΔV^r is the ground electronic energy of the reactant (V^r) corrected by an energy shift that arises because the angular constraint pushes the reactant away from its global minimum energy. As such, the gradient of the potential is not zero at the fixed-angle reactant minimum, requiring a coordinate shift by “completing the square” to quantize the vibrations. ΔV^\ddagger is defined analogously at the transition state. ΔV^r and ΔV^\ddagger are given by

$$\Delta V^r = V^r - \frac{1}{2} \sum_{i=1}^F \left(\frac{G_i^r}{\omega_i^r} \right)^2 \quad (2.8)$$

$$\Delta V^\ddagger = V^\ddagger - \frac{1}{2} \sum_{i=1}^{F-1} \left(\frac{G_i^\ddagger}{\omega_i^\ddagger} \right)^2 \quad (2.9)$$

where G_i^r is the mass-weighted gradient of the potential expressed in reactant normal modes for mode i , and likewise for G_i^\ddagger at the transition state.

An obvious difficulty of the present approach is the attempt to blend a normal mode picture of reactivity with a sudden approximation that fixes a nonlinear local mode. In particular, it remains difficult to project out the O–Al–O angle from the normal mode representations inherent in eqs 2.4, 2.5, 2.8, and 2.9. In effect we are double counting the angular motion, since the normal modes account for O–Al–O bending. To test the magnitude of error associated with this double counting, we compare below rate calculations using correct oxygen and aluminum masses in the central O–Al–O moiety, to those using very large masses, e.g., 10^6 au. If the results give reasonable agreement, we surmise that this double counting is not too serious an approximation. Nonetheless, we seek improved formulations of SC-TST that allow a more natural blending of normal mode analysis and local mode constraints.

The tunneling correction factor in eq 2.6 is the truncated-harmonic version of what Hernandez and Miller originally

published in ref 17. The parameter θ_0 is the maximum allowed generalized barrier penetration integral, which is associated with the ground state of reactants. As discussed in paper II, θ_0 is given by $\pi\Delta E_0/\hbar|\omega_F^\ddagger|$, where ΔE_0 is the ZPVE corrected barrier height given by

$$\Delta E_0 = \left(\Delta V^\ddagger + \sum_{i=1}^{F-1} \frac{\hbar\omega_i^\ddagger}{2} \right) - \left(\Delta V^r + \sum_{i=1}^F \frac{\hbar\omega_i^r}{2} \right) \quad (2.10)$$

We note that the expression for ΔE_0 given in eq 2.10 is generalized for normal-mode analyses away from true critical points, involving ΔV^r and ΔV^\ddagger instead of just V^r and V^\ddagger .

In the rigorously harmonic limit ΔE_0 goes to infinity, the first term in eq 2.6 vanishes when $k_B T > \hbar|\omega_F^\ddagger|/2\pi$, the upper limit of the integral extends to infinity, and the well-known harmonic limit is obtained: $\Gamma \rightarrow \alpha/\sin(\alpha)$ where $\alpha = \beta\hbar|\omega_F^\ddagger|/2$. As discussed in the Introduction, this harmonic expression becomes useless for temperatures at or below $T = \hbar|\omega_F^\ddagger|/2\pi k_B$. In paper I, we obtained an MP2/6-31G(d) barrier curvature of $|\bar{\nu}_F^\ddagger| = |\omega_F^\ddagger|/2\pi c = 1570 \text{ cm}^{-1}$ (c is the speed of light), which gives a harmonic divergence temperature of 360 K. However, by reintroducing the ground state of reactants, i.e., keeping ΔE_0 and hence θ_0 finite, we arrive at the truncated-harmonic theory given in eq 2.6. In addition to giving the correct high-temperature limit, i.e., $\Gamma \rightarrow 1$ as $T \rightarrow \infty$, the truncated-harmonic tunneling factor gives the following low-temperature limit:

$$\Gamma(T) \xrightarrow{T \rightarrow 0} \tilde{\Gamma}(T) = e^{\beta\Delta E_0} \cdot e^{-2\pi\Delta E_0/\hbar|\omega_F^\ddagger|} \left(1 + \frac{2\pi}{\beta\hbar|\omega_F^\ddagger|} \right) \quad (2.11)$$

It is noteworthy that at low temperatures, our formula for $\Gamma(T)$ becomes proportional to $e^{\beta\Delta E_0}$, hence eliminating the classical Arrhenius temperature dependence from $k^{\text{TST}}(T)$, as is well-known from both experiment and theory. Thus, our tunneling correction factor clearly exhibits the correct low and high temperature limits and hence provides a qualitatively reliable method for calculating quantum rate coefficients for nearly separable systems.

D. Summary of Computational Methods. Here we briefly summarize the computational methods applied in this article to study proton transfer in zeolites. We first choose a set of relevant O–Al–O angles for use in eq 2.1. These angles fall between 76° and 94° , because the reactant minimum occurs at $\phi = 93.8^\circ$, while the saddle point value is 78.4° .⁴ For each value of ϕ_j , we perform the electronic structure calculations described above to obtain V^r , $\{G_i^r\}$, and $\{\omega_i^r\}$ at the fixed-angle reactant minimum, as well as V^\ddagger , $\{G_i^\ddagger\}$, and $\{\omega_i^\ddagger\}$ at the fixed-angle transition state. Armed with these parameters, we evaluate $k(\phi_j)$ within SC-TST according to eqs 2.3–2.10. Finally, after repeating this process for all N_ϕ angles, we properly normalize $\rho(\phi_j)$ with eq 2.2 allowing the final rate calculation in eq 2.1.

III. Results and Discussion

In this section we describe the results of the computational strategy outlined above for modeling proton transfer in H–Y zeolite within the angular sudden approximation. We first discuss the angular dependence of V^r , ΔV^r , V^\ddagger , and ΔV^\ddagger resulting from the electronic structure calculations. We then describe the angular dependence of $k(\phi_j)$ and $\rho(\phi_j)$ for several temperatures. Finally, we report the temperature dependence of the full proton-transfer jump rate for comparison with both experimental data and our previous results reported in paper II.

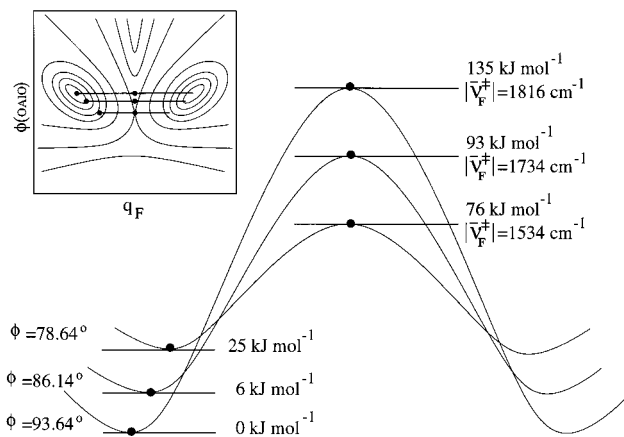


Figure 2. Schematic of fixed-angle proton jump paths showing results from electronic structure calculations for V^r , V^\ddagger and $|\bar{\nu}_F^\ddagger|$. Both the classical barrier height and the barrier curvature increase with the O–Al–O angle.

Figure 1 shows the detailed structure of our cluster model at the proton jump transition state for $\phi_j = 78.6^\circ$, which is very near the first-order saddle point for this system at 78.4° . The Si–O bond lengths in Figure 1 are larger than typical values in silicate materials (ca. 1.6 \AA) because the cluster is protonated. Figure 2 shows a schematic depiction of fixed-angle proton transfer double wells, labeled by our density functional theory results for V^r , V^\ddagger , and $|\bar{\nu}_F^\ddagger|$. In general, we find that both the classical barrier height and the barrier curvature increase as the angle increases from the saddle point value to the reactant minimum value (93.64°).

As discussed in section IIC, the SC-TST rate constants computed herein use shifted energies, ΔV^r and ΔV^\ddagger , rather than bare energies V^r and V^\ddagger . We also noted in section IIA that the zeolite is terminated with artificially massive hydrogen atoms. Unfortunately, because the difference between V^r and ΔV^r (and likewise for V^\ddagger and ΔV^\ddagger) involves the ratio between mass-weighted gradients and vibrational frequencies (cf. eqs 2.8 and 2.9), this difference is extremely sensitive to terminal atom mass effects. We find from our present calculations that the majority of the shift comes from normal modes associated with the (massive) terminal hydrogens, and that the shift can be as large as the classical barrier itself. When these modes are omitted from the sums in eqs 2.8 and 2.9, the shifts decrease by several orders of magnitude to negligible energies. This sensitivity to termination effects is one of the many unsatisfactory aspects of cluster modeling in computational materials science. The approach we adopt in the present study is to omit the terminal mode contributions to eqs 2.8 and 2.9, which is tantamount to ignoring the shifts entirely. To address this and other issues raised by cluster modeling, such as the role of long-range forces, we will report in a forthcoming publication the results of extended zeolite calculations,²⁷ using the embedded cluster method developed by Sauer and co-workers.²⁸

Parts a and b of Figure 3 show the angular dependence of $\rho(\phi)$, $k(\phi)$, and $\rho(\phi) \cdot k(\phi)$ at $T = 200$ and 588 K , respectively. The units of $k(\phi)$ are s^{-1} while those for $\rho(\phi)$ are radians^{-1} . As such, we scale $\rho(\phi)$ by the factors shown in Figure 3a,b to more clearly reflect the angular dependence of $\rho(\phi)$ and $\rho(\phi) \cdot k(\phi)$. As expected, $\rho(\phi)$ increases rapidly with ϕ as the angle approaches 93.8° , the value for the minimum energy reactant configuration. Alternatively, $k(\phi)$ decreases strongly with ϕ in Figure 3a,b; in both cases $k(\phi)$ decreases because the barrier height grows strongly with ϕ , as shown in Figure 2. For temperatures in the classical regime, such as $T = 588 \text{ K}$ in

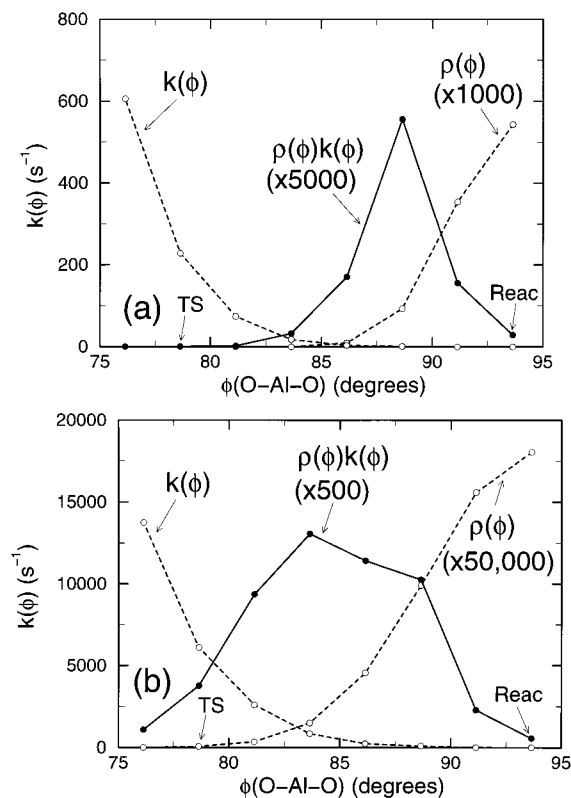


Figure 3. Angular dependence of $\rho(\phi)$, $k(\phi)$ and $\rho(\phi) \cdot k(\phi)$ at (a) $T = 200$ K and (b) $T = 588$ K. Curves involving $\rho(\phi)$ are scaled by the factors shown to display clearly the angular dependence. The peak angle and width of the dynamical distribution $\rho(\phi) \cdot k(\phi)$ decreases and increases with temperature, respectively.

Figure 3b, $k(\phi)$ decreases because increasing the barrier height slows the rate of activated barrier crossing. For temperatures in the quantum regime, such as $T = 200$ K in Figure 3a, the angular dependence of $k(\phi)$ can be understood as follows. The ground state tunneling probability is approximately given by $e^{-2\theta_0}$, where $\theta_0 = \pi\Delta E_0/\hbar|\omega_F^\ddagger|$ in our truncated-harmonic model. Figure 2 shows that both $(V^\ddagger - V^r)$ and $|\bar{v}_F^\ddagger|$ grow with ϕ ; the former trend decreases tunneling probabilities, while the latter increases them. Figure 2 also shows that $(V^\ddagger - V^r)$ grows more rapidly than does $|\bar{v}_F^\ddagger|$. As such, θ_0 grows with ϕ because the increasing barrier height dominates, causing tunneling probabilities to decrease strongly with ϕ , as shown in Figure 3a.

The “dynamical distribution” $\rho(\phi) \cdot k(\phi)$ peaks at 88.64° for $T = 200$ K, with a full width at half-maximum (fwhm) of 3.6° . This angular range includes neither the reactant angle (93.8°) nor the transition state angle (78.4°) but is closer to the reactant. This dynamical distribution signals the importance of paths far from the MEP, i.e., large curvature paths. Increasing the temperature to 588 K produces a dynamical distribution that peaks at 83.64° with a fwhm of 10.0° , now easily encompassing both the reactant and transition state angles. At low temperatures, we generally expect the dynamical distribution to focus on angles close to the value at the reactant minimum energy geometry. At high temperatures, we expect the distribution to broaden toward transition state geometries, validating the use of methods based on the minimum energy path (MEP).

Figure 4a shows the temperature dependence of $\rho(\phi) \cdot k(\phi)$ for all eight angles considered, over the temperature range 170 – 5000 K. The smaller angles show an extended Arrhenius temperature dependence because contracting the angle requires classical activation in our present model. The larger angles, on the other hand, exhibit clear non-Arrhenius temperature depen-

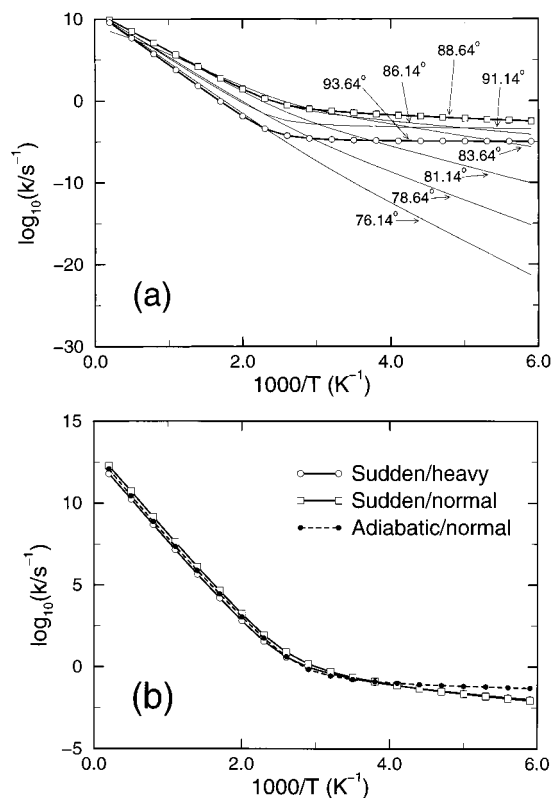


Figure 4. (a) Arrhenius plot of $\rho(\phi) \cdot k(\phi)$ for the 8 angles studied, showing that 88.64° is the most important angle for proton transfer over a wide temperature range, and that 10^{-5} s^{-1} is the low temperature limit of the sudden rate. (b) The completely averaged rate constants, showing surprisingly good agreement between the conventional SC-TST and sudden approaches in this temperature range.

dence because adopting these geometries requires minimal activation, so tunneling from these angles can occur at low temperatures. We note that the only angle that gives essentially no temperature dependence at low temperature is 93.64° (open circles in Figure 4a), which corresponds to the lowest energy ground state considered. The low-temperature rate constant for this angle plateaus at ca. 10^{-5} s^{-1} , which is the low-temperature limit when averaging over angles in the present theory, because all other angles carry a classical Boltzmann weight. We also note that in the temperature range 170 – 330 K, the most important O–Al–O angle for proton transfer is 88.64° (open squares in Figure 4a), which is consistent with the dynamical distribution shown in Figure 3a. For temperatures below 330 K, $\rho(88.64^\circ) \cdot k(88.64^\circ)$ remains in the range $10^{-2.5}$ to $10^{-1.3} \text{ s}^{-1}$.

As discussed in section IIC, our attempt to blend a normal mode picture of reactivity with a local mode sudden approximation introduces some double counting into the entropy portion of the rate calculation, which typically impacts the preexponential factor. By comparing our rate calculations with those where the central O–Al–O atoms are given extremely high masses, which essentially eliminates the double counting, we can determine its effect. In Figure 4b we show this comparison by plotting the temperature dependence of the completely averaged rate constants. Figure 4b shows essentially no difference between the sudden approximation with normal O–Al–O masses and that with artificially massive O–Al–O atoms; only a slight difference in the preexponential factor (as expected) can be seen at high temperatures.

We also compare in Figure 4b our present sudden approximation results with the MEP-based calculations reported in paper II. There is remarkably little difference between the sudden and

conventional SC-TST results, except at very low temperatures where a weak temperature dependence in the sudden rate remains. The sudden rate temperature dependence in the range 170–330 K arises because of the activated contraction of ϕ from 93.64° to 88.64°; this temperature dependence is virtually identical to that exhibited by $\rho(88.64^\circ) \cdot k(88.64^\circ)$ in Figure 4a. The fact that the sudden and conventional SC-TST rates are within an order of magnitude of each other in Figure 4b must be regarded as coincidence. Indeed, as discussed above, the low-temperature limit of the sudden rate is ca. 10^{-5} s^{-1} , which is several orders of magnitude lower than the conventional SC-TST rate plateau value. Nonetheless, the temperature range 200–1000 K is the most relevant for zeolite science. In this range the sudden and conventional SC-TST rates agree extremely well, and conventional SC-TST requires much less electronic structure input. It remains to be seen whether this agreement between the sudden and conventional SC-TST methods arises for other systems as well.

We close section III by comparing our results with experiment. As discussed in the Introduction, Sarv et al.¹⁹ used variable temperature MAS NMR to measure proton jump rates at 298, 478, 568, and 658 K, yielding an apparent activation energy of 61 kJ mol⁻¹. Because Sarv et al. did not measure proton jump rates over a sufficiently wide range or fine mesh of temperatures, they were unable to observe non-Arrhenius temperature dependence. Nonetheless, our results suggest that the temperature range 298–658 K overlaps significantly with the tunneling regime. Assuming an Arrhenius temperature dependence for measured proton transfer rates in the tunneling regime will underestimate the true ZPVE corrected barrier. We thus believe that the actual ZPVE corrected barrier may be significantly larger than the measured value of 61 kJ mol⁻¹. Indeed, our best electronic structure calculations yield 86.1 kJ mol⁻¹ for an isolated cluster and 97.1 kJ mol⁻¹ when approximately accounting for long-range interactions.²⁰ On the other hand, forcing an Arrhenius fit through our calculated conventional SC-TST rates at 298 K, 478, 568, and 658 K gives an apparent activation energy of 53.0 kJ mol⁻¹, which is in reasonable “agreement” with the experimental value of 61 kJ mol⁻¹. When we recalculate these proton jump rates using the present sudden approach, and subject these four rates to an Arrhenius fit, we obtain an apparent activation energy of 55.8 kJ mol⁻¹, in even closer “agreement” with experiment. The theoretical activation energy increases when using the sudden approximation because of the residual temperature dependence at low temperatures associated with contracting the O–Al–O angle. Approximating the effect of long-range forces should bring our result into even better “agreement” with experiment.²⁷

IV. Concluding Remarks

We have developed and applied an angular sudden approximation for modeling proton transfer in zeolites, using Miller’s semiclassical transition state theory (SC-TST) approach. We have parametrized the SC-TST calculations by performing B3LYP/6-311G(d,p) density functional theory calculations for paths with fixed O–Al–O angle in a cluster model of H–Y zeolite. We find that both the barrier height and barrier curvature increase with increasing angle, ϕ , from 78.6° (near the first-order saddle point) to 93.6° (near the reactant minimum energy geometry). We find that the classical barrier height increases with angle more rapidly than does the curvature, so that in our truncated-harmonic theory the ground state tunneling probability decreases strongly with ϕ . As a result of these trends, the range

of important angles for proton transfer, the so-called dynamical distribution, involves angles far from the saddle point angle at low temperatures (i.e., large curvature paths). The dynamical distribution broadens significantly at higher temperatures, encompassing the saddle point region.

The final temperature dependence of the proton jump rate within the sudden approximation shows surprisingly good agreement with that from conventional SC-TST, which is based on the minimum energy path as reported in paper II (ref 5). We attribute this in part to a coincidence that occurs in the temperature regime of interest, namely 200–1000 K, a coincidence that we do not expect will occur in other systems.

These calculations demonstrate the need for zeolite models beyond the cluster approximation,²⁷ as well as more natural ways to blend sudden and normal mode pictures of reactivity. Nonetheless, the calculations reported herein would not have been possible without the many seminal contributions to direct dynamics theory made over the years by Miller and co-workers.

Acknowledgment. We thank Prof. W. H. Miller for many years of encouragement, inspiration, and enlightening discussions regarding semiclassical rate theory. This work was supported by the National Science Foundation (CHE-9616019 and CTS-9734153), a Sloan Foundation Research Fellowship (BR-3844), and a Camille Dreyfus Teacher-Scholar Award (TC-99-041).

References and Notes

- (1) Eberly, P. E., Jr.; Kimberlin, C. N., Jr.; Miller, W. H.; Drushel, H. V. *Ind. Eng. Chem. Proc. Des. Dev.* **1966**, *5*, 193.
- (2) Corma, A. *Chem. Rev.* **1995**, *95*, 559.
- (3) Truong, T. N. *J. Phys. Chem. B* **1997**, *101*, 2750.
- (4) Fermann, J. T.; Blanco, C.; Auerbach, S. M. *J. Chem. Phys.* **2000**, *112*, 6779.
- (5) Fermann, J. T.; Auerbach, S. M. *J. Chem. Phys.* **2000**, *112*, 6787.
- (6) Ryder, J. A.; Chakraborty, A. K.; Bell, A. T. *J. Phys. Chem. B* **2000**, *104*, 6998.
- (7) Borgis, D.; Hynes, J. T. *J. Phys. Chem.* **1996**, *100*, 1118.
- (8) Lee, C.; Yang, W.; Parr, R. G. *Phys. Rev. B* **1988**, *37*, 785.
- (9) Becke, A. D. *J. Chem. Phys.* **1993**, *98*, 5648.
- (10) Krishnan, R.; Pople, J. A. *Int. J. Quantum Chem.* **1978**, *14*, 91.
- (11) Krishnan, R.; Frisch, M. J.; Pople, J. A. *J. Chem. Phys.* **1980**, *72*, 4244.
- (12) Miller, W. H.; Schwartz, S. D.; Tromp, J. W. *J. Chem. Phys.* **1983**, *79*, 4889.
- (13) Voth, G. A.; Chandler, D.; Miller, W. H. *J. Chem. Phys.* **1989**, *91*, 7749.
- (14) Miller, W. H.; Handy, N. C.; Adams, J. E. *J. Chem. Phys.* **1980**, *72*, 99.
- (15) Miller, W. H. *Faraday Discuss. Chem. Soc.* **1977**, *62*, 40.
- (16) Miller, W. H.; Hernandez, R.; Handy, N. C.; Jayatilaka, D.; Willets, A. *Chem. Phys. Lett.* **1990**, *172*, 62.
- (17) Hernandez, R.; Miller, W. H. *Chem. Phys. Lett.* **1993**, *214*, 129.
- (18) Bell, R. P. *Proc. R. Soc. A* **1935**, *148*, 241.
- (19) Sarv, P.; Tuherm, T.; Lippmaa, E.; Keskinen, K.; Root, A. *J. Phys. Chem.* **1995**, *99*, 13763.
- (20) Sauer, J.; Sierka, M.; Haase, F. In *Transition State Modeling for Catalysis*; Truhlar, D. G., Morokuma, K., Eds.; ACS Symposium Series No. 721; American Chemical Society: Washington, 1999; Chapter 28, pp 358–367.
- (21) Miller, W. H. *J. Chem. Phys.* **1975**, *62*, 1899.
- (22) Siebrand, W.; Smedarchina, Z.; Zgierski, M. Z.; Fernandez-Ramos, A. *Int. Rev. Phys. Chem.* **1999**, *18*, 5.
- (23) Szabo, A.; Ostlund, N. S. *Modern Quantum Chemistry: Introduction to Advanced Electronic Structure Theory*; McGraw-Hill: New York, 1989.
- (24) Frisch, M. J.; et al. *Gaussian98*, revision a.3; Gaussian Inc.: Pittsburgh, PA, 1998.
- (25) Rodriguez, A. *Vibr. Spectrosc.* **1995**, *9*, 225.
- (26) Messiah, A. *Quantum Mechanics*; John Wiley & Sons: New York, 1958.
- (27) Fermann, J. T.; Auerbach, S. M. **2000**.
- (28) Sierka, M.; Sauer, J. *J. Chem. Phys.* **2000**, *112*, 6983.